Applied Physics Letters

Hand-generated piezoelectric mechanical-to-electrical energy conversion plasma

Cite as: Appl. Phys. Lett. **117**, 093901 (2020); https://doi.org/10.1063/5.0018967
Submitted: 18 June 2020 . Accepted: 10 August 2020 . Published Online: 01 September 2020

Olivia K. Jaenicke, Federico G. Hita Martínez, Jinyu Yang, Seong-kyun Im, and David B. Go

Applied Physics Letters ARTICLE scitation.org/journal/apl

Hand-generated piezoelectric mechanical-to-electrical energy conversion plasma

Cite as: Appl. Phys. Lett. **117**, 093901 (2020); doi: 10.1063/5.0018967
Submitted: 18 June 2020 · Accepted: 10 August 2020 ·
Published Online: 1 September 2020

Olivia K. Jaenicke,[1] Federico G. Hita Martínez,[1] Jinyu Yang,[1] Seong-kyun Im,[1,2,a)] and David B. Go[1,3,a)]

AFFILIATIONS

[1]Department of Aerospace and Mechanical Engineering, University of Notre Dame, Notre Dame, Indiana 46556, USA
[2]School of Mechanical Engineering, Korea University, Seoul 02841, South Korea
[3]Department of Chemical and Biomolecular Engineering, University of Notre Dame, Notre Dame, Indiana 46556, USA

[a)]**Authors to whom correspondence should be addressed:** sim3@korea.ac.kr and dgo@nd.edu

ABSTRACT

A transient spark discharge is an atmospheric pressure plasma that has applications in pollutant removal, medicine, water treatment, agriculture, bactericides, and nanomaterial synthesis. Conventional methods of generating transient sparks at atmospheric pressure usually require a high voltage input at nanosecond pulses. Piezoelectric crystals offer a path to creating plasma devices that do not require a high voltage power supply to generate high voltage outputs; they directly transform mechanical energy into electrical energy. This work examines a manually-operated piezoelectric mechanical-to-electrical energy conversion plasma device. Electrical characterization of the plasma discharge generated by this device shows that it behaves as a transient spark, discharging 0.96 mJ over approximately 30 ns, with consistent behavior across multiple consecutive discharges. Although this specific device had a low mechanical-to-plasma energy conversion efficiency of 1.54%, the piezoelectric crystal resets to an equilibrium condition after approximately 8 μs, which suggests that it could be operated with a mechanical input of up to nearly 125 kHz. This work shows the potential of generating plasma in off-the-grid situations using piezoelectric crystals. One particular application of a piezoelectric plasma device is for *in situ* pollution mitigation or plasma-enhanced combustion, embedding such a device on the high-frequency oscillating or rotating components of internal combustion engines and turbomachinery.

It is well known that plasma-based technologies have applications across a wide variety of domains.[1] Transient spark and nanosecond-pulsed spark discharges are one form of laboratory plasma that have lately received significant attention. A transient spark discharge is a filamentary streamer-to-spark transition discharge generated by short, high voltage (∼5–10 kV) pulses and characterized by a short spark (∼10–100 ns), a high current peak (>1 A), and a low discharge energy (∼0.1–1 mJ per pulse).[2,3] A transient spark is initiated by a streamer, a filamentary path of ionized gas, that transitions to a spark once the streamer reaches the grounded electrode in the presence of the high voltage pulse. This produces an atmospheric pressure, non-equilibrium plasma with applications in pollutant removal,[4] medicine,[5,6] water treatment,[7] agriculture,[8] bactericides,[9] and nanomaterial synthesis.[10,11] One challenge limiting the application of transient spark and nanosecond-pulsed spark discharges is that they require power supplies that can deliver very high voltages on nanosecond time scales. As many of the applications noted above would find great use in environments outside the lab—such as on-board vehicular pollutant mitigation or medical therapeutics in disaster and relief areas—developing new approaches to generate these discharges could be very impactful.

Non-centrosymmetric crystals could form the basis of plasma devices that do not require a power supply; instead, they would utilize other forms of energy (thermal or mechanical) as input to produce a high electric field and subsequent gas breakdown, what we term "energy-conversion plasmas." For example, pyroelectric crystals produce very high surface electric fields when thermally cycled as their innate polarization increases or decreases, causing the surrounding gas to break down. Neidholdt and Beauchamp first used this thermal-to-discharge approach as an ionization source for mass spectrometry,[12] and we followed up on this concept to demonstrate the formation of stable corona-like discharges in atmospheric air.[13] Similarly, piezoelectric crystals can produce very high surface fields when undergoing mechanical deformation, and this principle is behind commercial spark devices such as gas grill igniters.[14] In an alternate configuration, piezoelectric transformer-based plasma devices, in which the piezoelectric crystal amplifies a low (∼10–30 V) input to sufficiently high

gains to produce a plasma, have also been demonstrated for a variety of applications[15–18] and are now commercial.[19,20] Here, we develop a manually-operated piezoelectric mechanical-to-electrical energy conversion plasma device that produces transient spark discharges. Characterization of the system shows the inherent promise of generating a plasma with only mechanical energy as the input, and we highlight potential useful applications, including utilizing inherent motion of mechanical systems and recovering vibrational waste energy.

We adapted a commercial piezoelectric spark igniter (PFLUSA Surefire Piezo 2 Wire Grill Igniter) and designed a rotational-to-linear mechanical actuator so that an individual can hand crank plasma ignition (Fig. 1). The spark igniter utilizes a lead zirconate titanate (PZT) piezoelectric ceramic, and a spring-loaded firing pin is compressed and released to make impact with the piezoelectric. A second restoring spring then recoils the firing pin to its equilibrium position [Fig. 1(a)]. The impact causes the piezoelectric to compress and creates a large polarization between the impact surface and the distal surface. While the igniter can be actuated a single time by manually compressing the firing spring and pin, to continuously actuate the plasma, a mechanism is required to repeatedly compress the firing spring and pin, allow them to reset, and compress them again.

We designed a hand cranked cam-and-follower snail drive to convert manually powered rotational motion to linear motion [Figs. 1(b) and 1(c)]. As the snail drive is rotated, it compresses the top cap of the igniter, generating a plasma, but upon further rotation, the notch in the snail shell-like shape [Fig. 1(c)] stops contact with the igniter and allows the restoring spring to reset the top cap to its initial position. As such, one plasma ignition can be completed per rotation of the snail drive. The top cap of the igniter must be compressed 12 mm to generate a spark, so this snail drive provides a maximum compression of 15.5 mm. It was found by measuring the stiffness of the two springs in the igniter that a force of 10 N is required to compress the springs and generate a spark. The crank handle was therefore positioned 35 mm from the center of rotation of the snail, delivering a torque of at least 0.35 N m. The snail was machined from a 12.7 mm (0.5 in.) thick high-density polyethylene (HDPE) and included a press fit bearing; the entire snail was press fit to a fixed 6.4 mm diameter shaft.

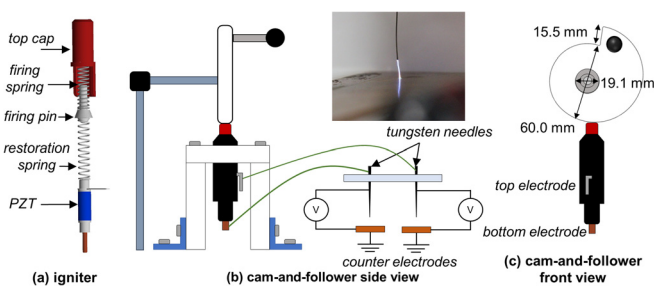

FIG. 1. (a) Exploded view of the piezoelectric igniter. (b) Side view schematic of the cam-and-follower snail drive and the electrical circuit to measure the transient output current and voltage. The resistors (shown in blue) are included in the circuit when measuring current. (c) Front view of the cam-and-follower snail drive. The snail is hand-cranked and designed to ensure adequate time for the firing pin to restore to equilibrium between each stroke. Pictured at the top is a typical spark produced at the tip of the needle.

When the snail is cranked, the impact of the firing pin compresses the piezoelectric to induce polarization such that electrodes connected to the two ends of the crystal [Fig. 1(c)] achieve high voltages of opposite polarity. High-voltage cables were soldered to the two electrodes, and these cables were connected to two 250 μm diameter, 50 mm long tungsten needles (Roboz Surgical 6064) that served as the electrodes for the transient sparks. The two needles were positioned 1.3 mm above two grounded counter electrodes (copper plates), as shown in Fig. 1(b). Upon each rotation, transient sparks form between each needle and their respective counter electrode, as shown in the photograph inset of Fig. 1, with each spark being of opposite polarity from the other.

Voltage measurements of the transient sparks were taken using high-frequency, high-voltage probes (Tektronix P6015A) connected to an oscilloscope (Tektronix DPO3012). Current measurements were conducted with a 100 Ω resistor in series with one of the counter electrodes, using a second high-frequency, high-voltage probe (Tektronix P6015). Oscilloscope sampling was triggered on the rising edge of channel 1, which collected the data for the top, negative electrode of the igniter. The data were acquired at a sampling rate of 10^8–10^9 Hz as noted below, collecting 10^4 data points for each experiment. To gather data for a single strike of the igniter, the snail was cranked once, and current and voltage data were simultaneously collected on one of the tungsten electrodes. This was then repeated to collect simultaneous current and voltage data for the other electrode. Measurements were also taken on both electrodes simultaneously to ensure the response was not affected by an interaction between the electrodes. To gather data for multiple strikes of the igniter, the snail was cranked a set number of times at approximately 2 Hz (120 RPM) and current and voltage data were recorded on the final strike of each series.

As shown in Fig. 2(a), the bottom, positive and top, negative electrodes of the igniter have similar voltage behavior. For each electrode, prior to ignition ($t < 0$ s), the voltage begins at $V = 0$ V and steadily increases in potential for about 6 μs due to the compression of the PZT crystal (pre-discharging stage). At $t = 0$ s, there is a sharp drop in the voltage of about ∼5 kV for both electrodes at the ignition of the transient spark (discharging stage). The current for each electrode begins at $i = 0$ A for $t < 0$ s and hovers between 0 and 2 A just before $t = 0$ s. This behavior reflects that seen by Janda *et al.*,[2] where it was characterized as the streamer ignition phase. The current rises at $t = 0$ s simultaneously with the voltage at the ignition of the transient spark, peaking at $i \sim -15$ A for the top, negative electrode [Fig. 2(b)] and $i \sim 30$ A for the bottom, positive electrode [Fig. 2(c)]. The discharging stage lasts for about 30 ns before dropping and showing a damped oscillation (ringing) behavior that continued for roughly 150 ns. This damped oscillation is also seen by Janda *et al.*[3] when generating transient sparks with a conventional power supply and is due to the parasitic inductance and internal capacitance of the system, which here includes the residual vibration of the PZT itself from the impact of the firing pin.

To determine the repeatability of the cam-and-follower snail drive, repeated actuations were conducted and current and voltage were measured during the last actuation in the series. As shown in Fig. 3, the electrical response of the discharge, in comparison to a single strike in Fig. 2, was unaffected by the number of repeated ignitions when measured after 5 strikes, 10 strikes, and 20 strikes. Each strike showed the same behavior with similar durations for the

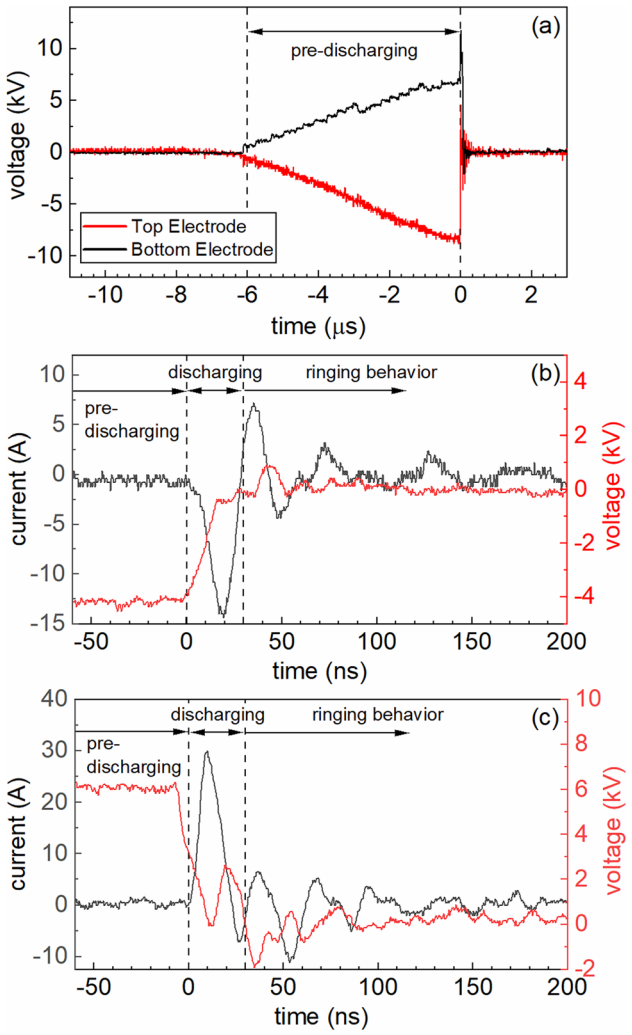

FIG. 2. Characteristic electrical response for a single transient spark ignition. (a) Voltage response of both electrodes on the scale of microseconds with a sampling rate of 2.5×10^8 Hz. Voltage and current response on the scale of nanoseconds of the (b) top, negative electrode and (c) bottom, positive electrode with a sampling rate of 2.5×10^9 Hz.

pre-discharging and discharging stages and ringing behavior. Small variations can be attributed to the natural stochasticity in the system. This shows that, at the frequency of actuation (~2 Hz), the PZT completely resets to an equilibrium state and there is negligible residual polarization.

To estimate the mechanical-to-plasma energy conversion efficiency of the system, we used a simplified model comparing the discharge power to the mechanical energy in the spring-driven firing pin. The energy in a single discharge was determined by integrating the instantaneous power $P(t)$ (the product of the current i and voltage V) over the duration of the spike in the discharging stage,

$$E_d = \int_{t_1}^{t_2} i(t)V(t)dt. \quad (1)$$

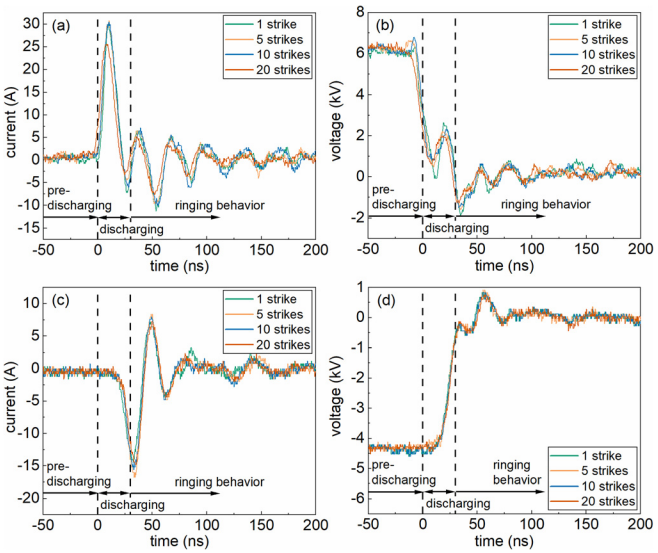

FIG. 3. (a) Current and (b) voltage response of the bottom, positive electrode and (c) current and (d) voltage response of the top, negative electrode over multiple strikes of the igniter. The data were recorded on the final strike of each series with a sampling rate of 2.5×10^9 Hz.

The bounds t_1 and t_2 were graphically determined as the edges of the power peak, as illustrated in Fig. 4. The average energy deposited in a single discharge of the igniter over 25 runs was found to be $E_d = 0.53 \pm 0.03$ mJ at 95% confidence for the top, negative electrode. Similar analysis for the bottom, positive electrode yielded $E_d = 0.43 \pm 0.03$ mJ. This energy value is consistent with the findings of others,[2,3] where the discharged energy in a single transient spark pulse was found to be ~0.1–1 mJ per pulse.

The mechanical energy of the cam-and-follower snail drive was estimated by the potential energy in the spring of the firing pin using

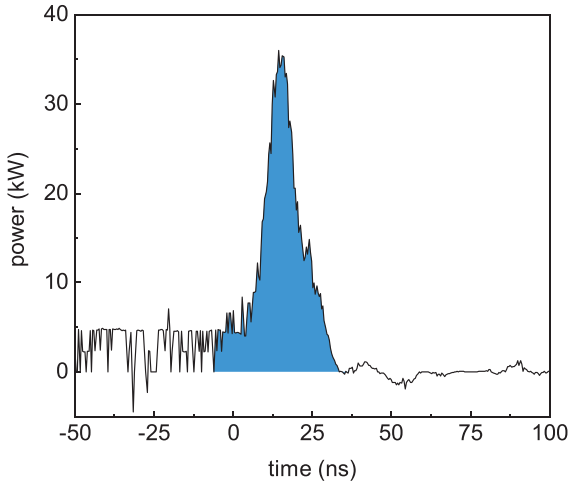

FIG. 4. Representative plot of power as a function of time for a single ignition. The shaded area shows the power in one discharge and was integrated to determine the energy deposited in one discharge.

$$E_p = \frac{1}{2}kx^2. \quad (2)$$

The spring constant, k, was found by pulling the spring with a known force, $F = 2.60 \pm 0.05$ N, and measuring its displacement, resulting in a value of $k = 867 \pm 25$ N/m. During impact, the displacement of the spring was directly measured to be $x = 12 \pm 0.5$ mm, such that the spring's potential energy is $E_p = 62.4 \pm 4.1$ mJ. The mechanical-to-plasma energy conversion efficiency is simply the ratio of these two energies, $\eta = (E_{d,top} + E_{d,bottom})/E_p$, and for this configuration, the mechanical-to-plasma energy conversion efficiency was estimated to be $\eta = 1.54 \pm 0.12\%$.

Overall, the designed system is relatively inefficient; less than 2% of the mechanical energy stored in the spring of the firing pin manifests itself in plasma formation. Furthermore, this estimate corresponds to the maximum possible efficiency as it does not account for non-idealities in the components of the cam-and-follower or ignitor (e.g., friction), inelastic behavior during the impact of the firing pin, or losses in the electrical connections and wires. Fundamentally, the inefficiency in the mechanical-to-plasma conversion can largely be attributed to two factors—the incomplete extraction of electrical energy from the PZT crystal, including electrical dissipation and energy returning back to mechanical form through the converse piezoelectric effect, and the losses in generating the spark discharge.[21–23] However, what the measurements do show is the inherent promise of the system. Careful inspection of Fig. 2(a) shows that the polarization of the PZT recovers on the order of 2 μs after the spark initiates and that the total time from the initial response prior to ignition through recovery is 8 μs, noting that this does not account for the time for the recoil spring to reset the firing pin to equilibrium. This suggests that in principle, with optimized mechanical design, this PZT crystal could be actuated as fast as 125 kHz and still operate successfully. A human-powered system, such as an optimized hand crank system, can only achieve a maximum cycling cadence of 126 RPM (2.1 Hz) over a sustained period of time.[24] Even if the crank were to be actuated with a geared bicycle, the cadence would be only ~100 RPM (1.67 Hz) for a professional cyclist,[25] which would correspond to 3 strikes per second. This might be useful for short-term plasma operation, such as purifying a small volume of water, but not realistic for the longer times needed to achieve the same outcomes as conventional high-voltage power supply-based systems.

Greater promise likely comes recovering the waste energy of mechanical systems that naturally operate at frequencies similar to the maximum achievable by such a piezoelectric plasma device or conventional pulsed power supply. For example, internal combustion engines and turbomachinery have oscillating and rotating components that regularly operate at frequencies of $\sim 10^1$ Hz ($\sim 10^3$ RPM) and 10^2–10^3 Hz (10^4–10^5 RPM), respectively.[26,27] As transient sparks have been shown to be useful for both enhanced combustion[28,29] and mitigation of pollutants,[4] one can envision a system where these types of devices are embedded into the design of the oscillating or rotating machinery or other vibrating components for *in situ* energy-harvested plasma-enhanced combustion and/or exhaust treatment.

This work is based on support from the National Science Foundation under Award No. PHY-1804091. Seong-kyun Im was supported by the National Research Foundation of Korea (NRF) grant funded by the Korea government (MSIT) under Award No. NRF-2020R1C1C1006837.

DATA AVAILABILITY

The data that support the findings of this study are available from the corresponding author upon reasonable request.

REFERENCES

[1]I. Adamovich, S. D. Baalrud, A. Bogaerts, P. J. Bruggeman, M. Cappelli, V. Colombo, U. Czarnetzki, U. Ebert, J. G. Eden, P. Favia, D. B. Graves, S. Hamaguchi, G. Hieftje, M. Hori, I. D. Kaganovich, U. Kortshagen, M. J. Kushner, N. J. Mason, S. Mazouffre, S. M. Thagard, H.-R. Metelmann, A. Mizuno, E. Moreau, A. B. Murphy, B. A. Niemira, G. S. Oehrlein, Z. L. Petrovic, L. C. Pitchford, Y.-K. Pu, S. Rauf, O. Sakai, S. Samukawa, S. Starikovskaia, J. Tennyson, K. Terashima, M. M. Turner, M. C. M. van de Sanden, and A. Vardelle, J. Phys. D **50**, 323001 (2017).
[2]M. Janda, Z. Machala, A. Niklová, and V. Martišovitš, Plasma Sources Sci. Technol. **21**, 045006 (2012).
[3]M. Janda, V. Martišovitš, and Z. Machala, Plasma Sources Sci. Technol. **20**, 035015 (2011).
[4]Z. Machala, M. Morvová, E. Marode, and I. Morva, J. Phys. D **33**, 3198 (2000).
[5]T. von Woedtke, S. Reuter, K. Masur, and K.-D. Weltmann, Phys. Rep. **530**, 291 (2013).
[6]A. A. Fridman and G. G. Friedman, *Plasma Medicine* (John Wiley & Sons Chichester, UK, 2013).
[7]P. Bruggeman and C. Leys, J. Phys. D **42**, 053001 (2009).
[8]M. Ito, J.-S. Oh, T. Ohta, M. Shiratani, and M. Hori, Plasma Process. Polym. **15**, 1700073 (2018).
[9]Z. Machala, B. Tarabova, K. Hensel, E. Spetlikova, L. Sikurova, and P. Lukes, Plasma Process. Polym. **10**, 649 (2013).
[10]D. Dobrynin, R. Rakhmanov, and A. Fridman, J. Phys. D **52**, 455502 (2019).
[11]D. Mariotti and R. M. Sankaran, J. Phys. D **43**, 323001 (2010).
[12]E. L. Neidholdt and J. L. Beauchamp, Anal. Chem. **79**, 3945 (2007).
[13]M. J. Johnson, J. Linczer, and D. B. Go, Plasma Sources Sci. Technol. **23**, 065018 (2014).
[14]Y. K. Tan, K. Y. Hoe, and S. K. Panda, in IEEE International Conference on Industrial Technology (2006), pp. 1711–1716.
[15]M. J. Johnson, D. R. Boris, T. B. Petrova, and S. G. Walton, IEEE Trans. Plasma Sci. **47**, 434 (2019).
[16]M. Teschke, Contrib. Plasma Phys. **49**, 614 (2009).
[17]M. J. Johnson and D. B. Go, J. Appl. Phys. **118**, 243304 (2015).
[18]J. Yang, S.-K. Im, and D. B. Go, Plasma Sources Sci. Technol. **29**, 045016 (2020).
[19]H. Itoh, K. Teranishi, and S. Suzuki, IEEE Trans. Plasma Sci. **30**, 124 (2002).
[20]H. Itoh, K. Teranishi, and S. Suzuki, Plasma Sources Sci. Technol. **15**, S51 (2006).
[21]Z. Yang, A. Erturk, and J. Zu, Extreme Mech. Lett. **15**, 26 (2017).
[22]J. Liang and W.-H. Liao, Smart Mater. Struct. **20**, 015005 (2011).
[23]S. Zhong, N. Miao, Q. Yu, and W. Cao, J. Electrost. **73**, 97 (2015).
[24]C. Krämer, L. Hilker, and H. Böhm, Eur. J. Appl. Physiol. **106**, 749 (2009).
[25]A. Lucia, J. A. Hoyos, and J. L. Chicharro, Med. Sci. Sports Exerc. **33**, 1361 (2001).
[26]J. W. Heffel, Int. J. Hydrog. Energy **28**, 1285 (2003).
[27]C. Zwyssig, J. W. Kolar, W. Thaler, and M. Vohrer, in Fourtieth IAS Annual Meeting, Conference Record of the 2005 Industry Applications Conference (2005), Vol. 1, pp. 253–260.
[28]C. D. Cathey, T. Tang, T. Shiraishi, T. Urushihara, A. Kuthi, and M. A. Gundersen, IEEE Trans. Plasma Sci. **35**, 1664 (2007).
[29]D. Alderman, C. Tremble, D. Singleton, J. Sanders, and C. Jiang, "Effects of pulse rise time and repetition frequency on nanosecond pulsed plasma ignition for combustion," Plasma Res. Express (published online, 2020).